Improved diurnal interpolation of Earth radiation budget observations using correlative ISCCP cloudiness data

Martial Haeffelin Robert Kandel
Claudia Stubenrauch
Laboratoire de Météorologie Dynamique

September 4, 1996

DRAFT VERSION

Abstract

The Earth radiation budget experiment (ERBE) was developed to provide a complete temporal and spatial coverage of the solar reflected and Earth emitted radiation. ERB measurements were resumed in 1994 by the Scanner for Radiation Budget (ScaRaB) mission on a single satellite. Due to sparse temporal sampling, diurnal variations must be accounted for in order to establish accurate unbiased daily and monthly mean radiant exitance. When the ERBE diurnal interpolation algorithm is used alone, large discrepancies are shown between monthly mean radiative flux of single and multi-satellite measurements. We extend the algorithm by accounting for diurnally varying cloud cover using ISCCP monthly mean data. Significant improvements are found in regions where clouds have a pronounced diurnal cycle. Further improvements are obtained by additionally taking into account diurnal variations of cloud properties such as optical thickness using either ISCCP cloud radiance data or a cloud classification. These approaches require the development of directional models to represent the angular dependence of the cloud albedo corresponding to the ISCCP cloud scene identification.

1 Introduction

The components of the Earth Radiation Budget (ERB) are the solar reflected flux (radiant exitance) and the thermal flux emitted by the Earth-Atmosphere system. The components of the ERB are monitored from broad band channels on board satellites. Among Earth observing satellites, both low orbit platforms and geostationary satellites will be considered here. The choice between these two types of platforms involves compromises in spatial and

temporal coverage, in resolution and sampling characteristics, in relation with the type of instrumental technology used.

Because ERB missions using polar orbiting platforms have limited spatial and temporal sampling, algorithms were developed in order to correctly account for the diurnal variability of the Earth's radiation in computing daily and monthly mean radiative fluxes. Determining radiative fluxes at the top of the atmosphere from satellite measured radiances requires hypotheses concerning the anisotropy of the Earth radiative field. In [1] it is shown that the most important factor for variability of this anisotropy is certainly the variability of cloud properties. In the Earth Radiation Budget Experiment (ERBE), described in [2], angular dependence models were developed to represent this anisotropy. This work can be found in [3, 4].

The first part of this paper presents the time averaging algorithm developed for ERBE for the shortwave (SW) spectral domain. The weaknesses of this algorithm are stressed and improved versions are proposed by complementing ERBE data with correlative measurements from the geostationary satellites.

2 The ERBE time averaging procedures

On global and zonal spatial scales, for quantities averaged yearly, seasonally, or monthly, the variability of the Earth's radiative field is driven predominantly by the annual cycle of the Earth-sun distance and the motion of the subsolar point relative to the equator. However, since satellites can not monitor all parts of the Earth simultaneously, attempts to determine monthly and seasonal means implies modelling diurnal variations of the Earth's radiative field at the regional level.

2.1 Directional models

To model the diurnal variability of the reflected solar radiation implies taking into account the variations of both the incident energy and the fraction which is reflected. The diurnal variation of the incident solar radiation is indeed very pronounced but can be accurately computed. The solar-zenith-angle dependence of the albedo,

$$A(\theta_0) = \frac{M_r(\theta_0)}{E_0(\cos\theta_0)}, \tag{1}$$

where M_r is the shortwave radiant exitance (SWRE), E_0 is the solar constant corrected for the variations of the Earth-sun distance, and θ_0 is the solar zenith angle, is assumed to follow directional models

$$\delta(\theta_0) = \frac{A(\theta_0)}{A(\theta_0 = 0)}, \tag{2}$$

given for each scene types. Figure 1 shows directional models, expressed in terms of albedos, for the geographical scene type *ocean* and *land* corresponding to the cloud types defined in the ERBE scene identification algorithm [1]. The data in Figure 1 is issued from [5].

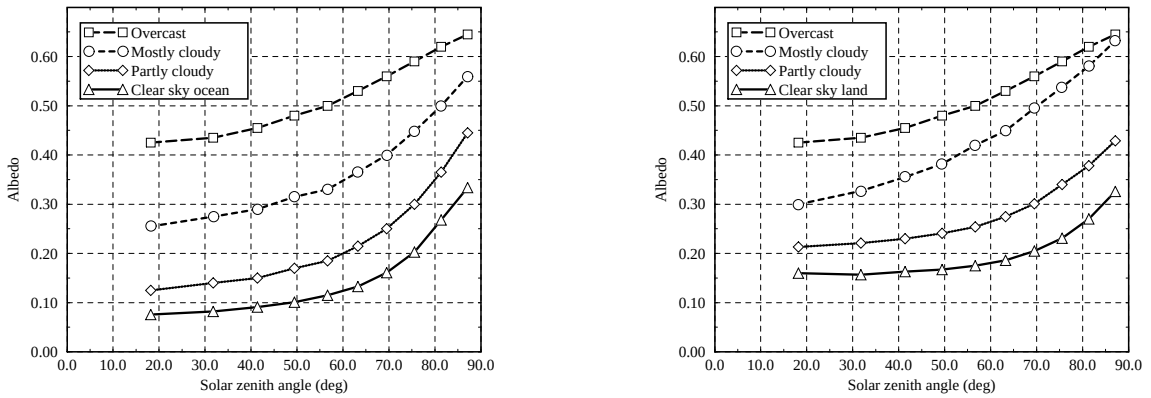

a) b)

Figure 1: ERBE angular directional model regional albedo as a function of the solar zenith angle for various scene types. The geographical type of the underlying surface is (a) *ocean* and (b) *land*.

2.2 Temporal interpolation and extrapolation algorithm in the SW domain

The SWRE for a given region and at a given time t is defined as

$$M_{SW}(t) = E_0(t)\mu(t)\sum_{i=1}^{4}\alpha_i(t)f_i(t), \tag{3}$$

where $\mu(t)$ is the cosine of the solar zenith angle, and $\alpha_i(t)$ and $f_i(t)$ are the albedos and normalized fractions of the four types of cloud cover for that region, respectively. The spatial resolution of an ERBE region is 2.5° by 2.5°.

To compute a radiant exitance $M_{SW}(t')$ from the measurement $M_{SW}(t_{obs})$, Equation (3) is applied at time t' and t_{obs}. By eliminating $E_0(d)$ between the two equations, $M_{SW}(t')$ becomes

$$M_{SW}(t') = \frac{\mu(t')}{\mu(t_{obs})}\,\frac{\sum_{i=1}^{4}\alpha_i[\mu(t')]f_i(t')}{\sum_{i=1}^{4}\alpha_i[\mu(t_{obs})]f_i(t_{obs})}\,M_{SW}(t_{obs}). \tag{4}$$

where $\alpha_i[\mu(t)]$ is here an albedo given by the directional models. Variations of $f_i(t)$ are not modelled, which is equivalent to considering the meteorology to be constant during the day. Variations of cloud properties are only taken into account if several measurements are performed during the day. In such a case, the SWRE is computed as a time weighted average of the two surrounding measurements. This weighting scheme assumes that the observed scene fraction change linearly with time from one observed set to the next.

2.3 Hypotheses of the algorithm and implications

The hypotheses are the following:

1. Radiance measurements are obtained with very low uncertainty,
2. Scene identification is correctly performed by the inversion subsystem, which uses bi-directional models and a maximum likelihood estimation (MLE) technique, descibed in [1],
3. Variations of the albedo with the solar zenith angle are represented by directional models, which are related to the bi-directional models,
4. Cloud cover type fractions at time t' are identical to that at time t_{obs}.

Errors implied by these hypotheses can be defined as follows:

1. The radiance uncertainty can propagate through the secondary data interpretation,
2. A random error due to the uncertainty of scene identification,
3. A random error, or a bias, due to angular sampling of measurements,
4. A random error, or a bias, due to particular diurnal cycles of cloudiness.

Errors in items 2 and 3 are inherent in the MLE technique and inaccuracies in the bi-directional models. In this paper we focus on issues related to diurnal cycle sampling.

2.4 Temporal sampling problems and subsequent biases

In [1] it is stated that flux measurements over short periods of time can be obtained but with significant uncertainty. The logic behind the ERBE time and space algorithm is that since errors often are random, the error of an averaged value will always be less than the sample value errors. This indeed is correct if errors are truly random and if sampling is not biased in any way. However, if errors are biased and sampling not complete, averaging will not allow errors to be reduced.

It appears from previous missions that a single-satellite system would not be satisfactory to determine the ERB [6]. To enhance spatial and temporal sampling, ERBE was developed in a multi-satellite approach. During most of the mission, at least two satellites were operational simultaneously.

At the regional scale, the daily meteorology may appear as a random phenomenon. Indeed this assumption is implicit in the ERBE monthly regional products, presumed to be more accurate than instantaneous pixel or daily regional fluxes, as a result of averaging out of random errors. However, several studies [7, 8] show that over large parts of the globe strong diurnal cycles of meteorology can remain over several days, weeks or even months. Considering the sparse temporal sampling performed by low orbit satellites, these remaining meteorological structures can induce very significant biases in the observed radiometric data.

Though meteorological phenomena are often well known and well described, quantitative data are not necessarily available to take them into account in budgeting the Earth's radiation. Therefore biases encountered at the regional and diurnal scales are propagated without attenuation through the computation of monthly averaged quantities.

2.5 Monthly means derived from single-satellite measurements

To study the impact of sparse temporal sampling on monthly mean products, ERBE inversion algorithms are applied separately to three single-satellite data sets. Single satellite results are compared to multi-satellite results, which are monthly mean products obtained by treating all the data sets together. December 1986 data were used since it is the only complete month for which the three ERBE satellites were operational simultaneously.

2.5.1 Oceans covered by low stratiform clouds

Stratocumulus clouds have a very extensive cover, in the order of hundred kilometers, and are usually considered as optically thick. They are found at low altitudes, i.e. below 2000 meters. In general, stratocumulus clouds are more reflective than the underlying surface and thus increase significantly the planetary albedo. Because of their low altitude, these clouds have a temperature close to that of the underlying surface; as a result they modify only weakly the thermal radiation to space. The combination of the two effects implies that the Earth radiation budget is very sensitive to the amount of stratocumulus clouds in the atmosphere.

Stratocumulus clouds are primarily found over the Earth's oceans [9] in the eastern part of the Southern and Northern Pacific as well as in the eastern part of the Southern Atlantic. Stratocumulus clouds are also found in the eastern part of subtropical oceanic highs where the wind blows from middle latitudes towards the intertropical convergence zone (ITCZ).

Initially we focused our interest on a stratocumulus region above the ocean west of the Namibian coast. Figure 2(a) shows the time sampling of the three ERBE satellites above this region for the month of December 1986. Note that NOAA-9 and NOAA-10 are sun-synchronous orbiters while ERBS has an orbit precessing through 12 hours of local time in 36 days.

A stratocumulus region is an interesting case study because the meteorological activity is very important and quite repetitive when considering time periods in the order of one month. Figure 3(a) shows monthly mean diurnal cycles of cloudiness and albedo issued from ISCCP stage C2 data. The albedo is derived from optical thickness data.

The cloud cover as well as the optical thickness develop during the night due to thermal radiative cooling at the cloud top. Maximum cloudiness and albedo occur in the vicinity of sunrise. As soon as solar heating starts stratiform convection decreases and clouds dissipate.

Figure 4(a) shows monthly mean diurnal cycles of the SWRE in that region for the month of December 1986. The solid line represents the diurnal cycle obtained from the multi-satellite data set. Using NOAA-10 sampled data alone clearly overestimates the diurnal

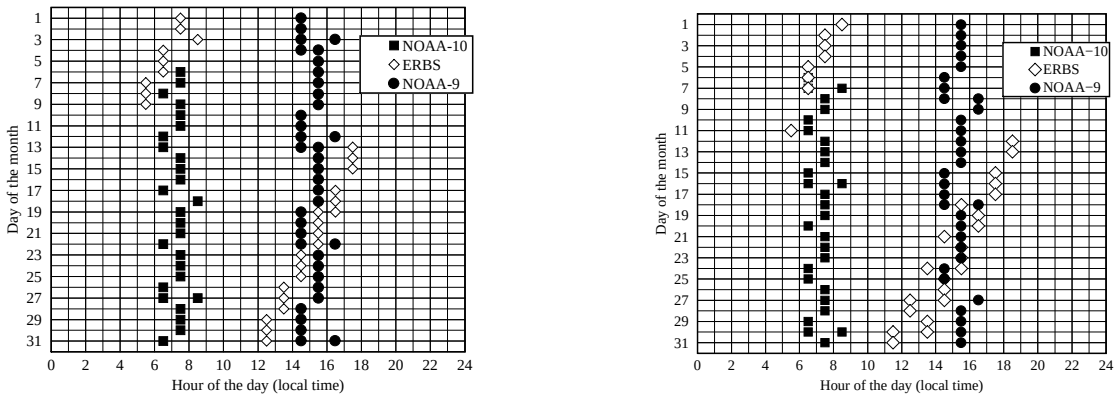

Figure 2: Temporal sampling by the three ERBE satellites. December 1986; (a) 20°S, 5°E; (b) 20°S, 20°E.

cycle while NOAA-9 and ERBS sampled data significantly underestimate it. This is easily understood by recalling simultaneously the diurnal cycles of cloudiness and albedo and the sampling hours of the three satellites. NOAA-10 samples in the morning hours shortly after sunrise during maximum cloudiness. Since stratocumulus clouds have a stronger albedo than the underlying marine surface, morning measurements will tend to monitor large radiant exitances. Because cloudiness is lower at any other time of the day, deriving a diurnal cycle from morning fluxes produces overestimated values. NOAA-9 samples at a time of the day when cloudiness is minimum. This produces underestimated SWRE diurnal cycle. The absolute difference between NOAA-9 and NOAA-10 monthly SWRE is greater than 70 W/m^2, which corresponds to a relative difference above 50 percent. ERBS sampled data produce results similar to NOAA-9 results. In Figure 2 we see that for two-thirds of the month, sampling was similar with the two satellites. In addition, a closer look at the daily cycles of cloudiness reveals low amplitude cycles during the first week of the month.

2.5.2 Land covered by convective clouds

This region is located on the African continent, in Northern Namibia, about 500 km East of the Atlantic coast. The region is centered on 20°S in latitude and 20°E in longitude.

The cold currents in the ocean along the coast of Namibia imply a cold and dry climate. The climate is typically semi-arid with warm days and cool nights. The cloud cover varies strongly along the day, as shown in Figure 3(b). The cloud cover is minimum around sunrise usually composed of optically thin high-altitude clouds. Radiative heating of the surface creates the conditions for rising air in which clouds develop. Cumulus clouds tend to develop in the morning and as the convective activity intensifies, vertically developed and optically thick cumulonimbus clouds obscur the sky. This region is at the same latitude as the region

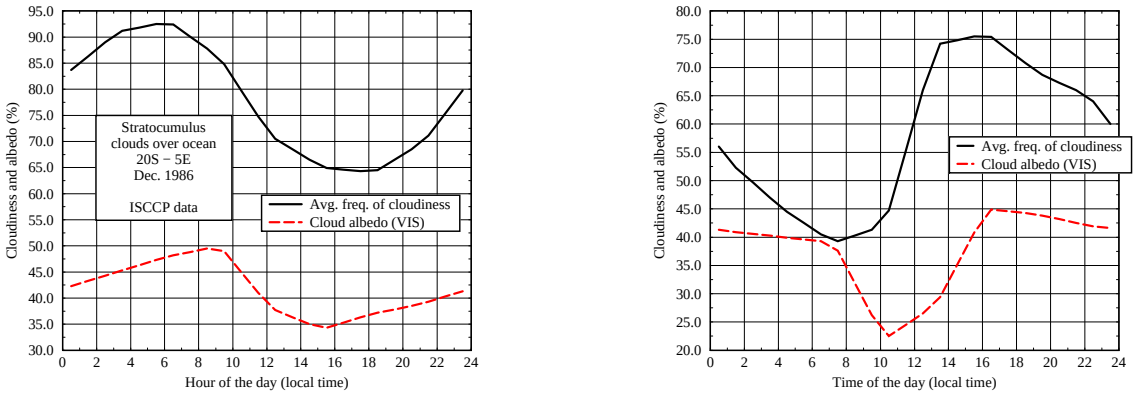

b)

Figure 3: Monthly mean diurnal cycles of cloud cover and cloud albedo. ISCCP C2 data; December 1986; (a) 20°S, 5°E; (b) 20°S, 20°E.

described in Section 2.5.1 which implies that the temporal sampling is similar, as is shown in Figure 2(b).

Figure 4(b) shows diurnal cycles of solar reflected fluxes derived from observations made by ERBE satellites. Here NOAA-10 derived fluxes are lower than the ones computed from NOAA-9 measurements because of the convective development of clouds in the afternoon. The difference in the monthly mean value of the flux between NOAA-9 and NOAA-10 is about 60 W/m^2 or 40 percent relative. The monthly mean flux computed from ERBS measurements is less than 5 W/m^2 away from that derived from the three satellites, but the shape of the diurnal cycle does not take into account the disymetry between the morning and afternoon fluxes. It is interesting to note that the combination of ERBS measurements with the diurnal pattern of the meteorology is much more successful in producing an accurate monthly mean flux than for the stratocumulus region. This is a coincidence for this particular region at this particular time of the year. With different times of observation during this month the different meteorological conditions were sampled uniformely which produced a monthly mean close to that derived from three or more measurements every day.

2.5.3 Global analysis

There are different approaches to study the impact of temporal sampling on monthly mean fluxes. Single-satellite data sets can be compared either to each other or to multi-satellite data sets.

2.5.3.1 Single- and multi-satellite products In Sections 2.5.1 and 2.5.2, it was shown that monthly diurnal cycles and monthly averages of the reflected solar flux can vary considerably depending on the number of measurements available each day. This effect is strongly

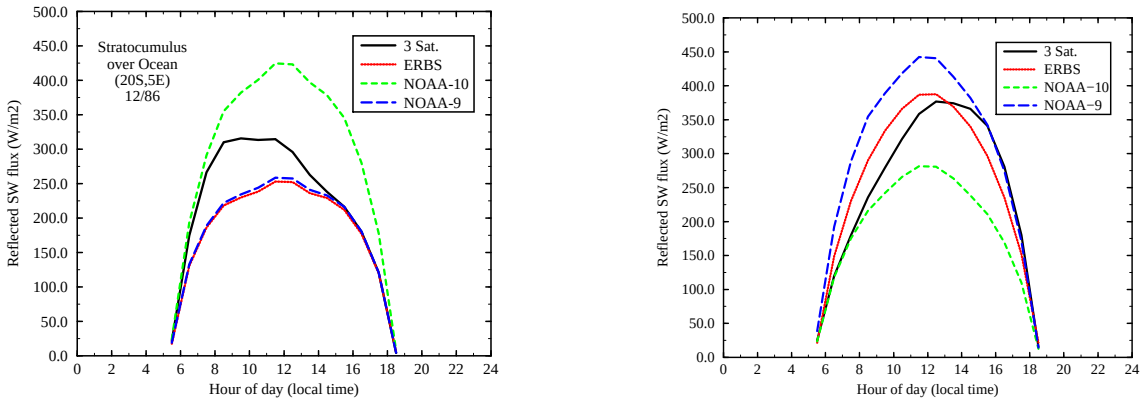

Figure 4: Monthly mean diurnal cycles of SW reflected flux based on single- or multi-satellite data. Results obtained from ERBE original data. December 1986; (a) Ocean, 20°S, 5°E; (b) Land, 20°S, 20°E.

correlated with the meteorological conditions which occur in these regions. Results will be very different according to surface type and latitude because these two parameters have a large influence on the type and variability of the cloud cover.

Figure 5 shows zonal averages of the difference between single- and multi-satellite derived reflected solar flux. These data concern ocean regions only. Figure 5(a) represents an average value of difference for each latitude band and Figure 5(b) its standard deviation.

For latitude between 20°S and 50°S, Figure 5(a) shows clearly that these regions are characterized by meteorological phenomena which have a strong disymetry between morning and afternoon. The strong negative bias associated with NOAA-10 data and the equally strong positive bias associated with NOAA-9 measurements indicate that the cloud cover must be systematically more important in the morning than in the afternoon. In addition, in the Northern hemisphere, part of the bias associated with NOAA-10 can be attributed to insolation conditions close to the terminator.

The bias for latitudes included between the equator and 20°S is very close to zero. This does not imply that regional monthly means derived from single-satellite data sets are close to multi-satellite products. This lack of bias is simply due to compensation of negative and positive bias of different longitudes. Indeed, the standard deviation, shown in Figure 5(b), are very large for these latitudes. The very large differences are found for instance in tropical ocean regions which are covered by large decks of stratocumulus clouds. It is worth noting that for ERBS, the standard deviation increases over the whole range of latitude from 50°N to 50°S.

Figure 6 represents zonal averages of the difference between single- and multi-satellite products over land regions. ERBS provides zonal averages without significant bias, NOAA-10 data show a positive bias and NOAA-9 products a negative one for the entire range of

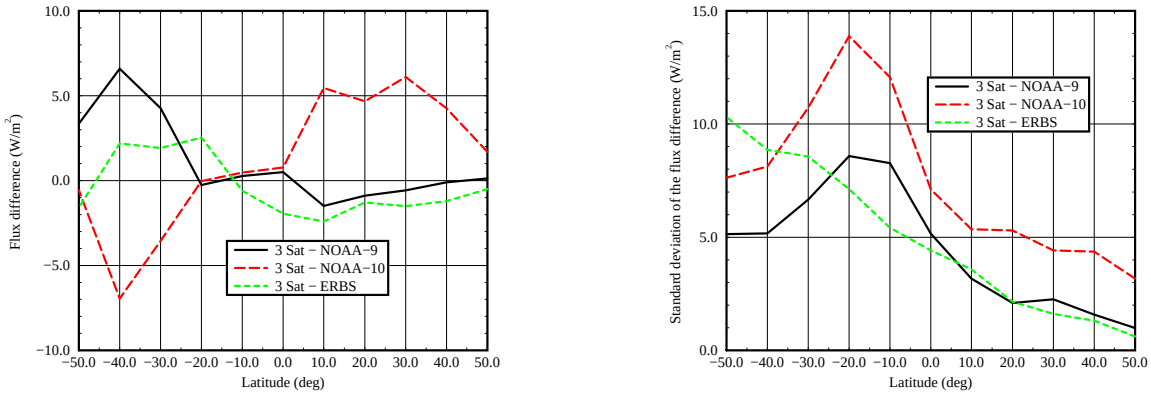

a) b)

Figure 5: (a) Mean and (b) standard deviation by latitude of the difference between single- and multi-satellite derived monthly mean reflected solar fluxes over ocean regions in december 1986. The zonal means are computed for 10° intervals.

latitude considered. NOAA-10 and NOAA-9 curves are almost perfectly the mirror image of each other. One can easily imagine a horizontal symetry line located approximatively at 2.5 W/m^2. This symetry is a sign that meteorological phenomenon on continents are radically different in the morning than in the afternoon.

The standard deviations, shown in Figure 6(b), reveal similar patterns for the three satellites, the largest values being associated with NOAA-10. For each satellite, the most significant standard deviations are found in the Southern hemisphere, close to 20°S. This latitude receives the maximum insolation of the planete. The activity of the cloud cover is governed in parts by energy exchanges such as radiative cooling at night and radiative heating during the day, which implies that the larger the insolation, the stronger the meteorological phenomenon.

2.5.3.2 Difference between NOAA-9 and NOAA-10 To study the impact of sparse temporal sampling on ERB results, we apply this analysis to all regions of the globe. The parameter of comparison becomes the monthly mean SWRE instead of the diurnal cycle for evident practical reasons. Figure 7 shows the relative difference in SWRE between NOAA-9 and NOAA-10 sampled data.

Negative values, shown in black and dark grey, represent regions in which NOAA-9 sampled data produced significantly lower monthly mean SWRE than NOAA-10 sampled data. Positive values for which NOAA-9 produces higher fluxes than NOAA-10 are shown in light grey. Regions drawn in white represent either lack of data or unsignificant differences between the two data sets.

Large negative values appear clearly in regions known for low level cloudiness activity during the boreal winter. These regions are principally covered by subtropical marine stratus

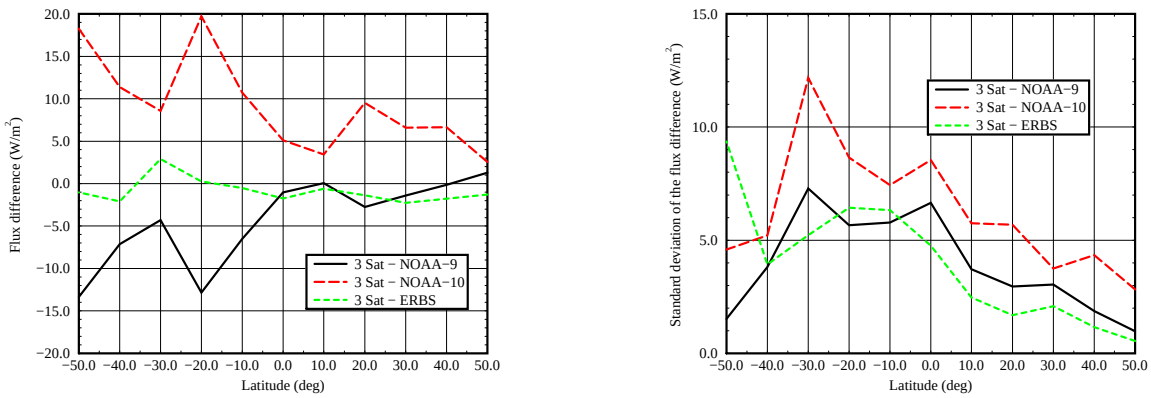

a) b)

Figure 6: (a) Mean and (b) standard deviation by latitude of the difference between single- and multi-satellite derived monthly mean reflected solar fluxes over land regions in december 1986. The zonal means are computed for 10° intervals.

clouds. They are located off the African coast, East of Namibia, off the South American coast, East of Peru, as well as South of the Australian coast and South of Polynesia. Large positive values are found on continents boarding these subtropical marine regions such as Angola and Namibia in Africa, Peru and Chili in South America, and parts of Australia.

In addition to the large patterns previously described one can see that an extensive part of the globe shows relative differences well above 10 percent. The mean difference for the globe is close to zero but the standard deviation is around 15 percent. Maximum relative difference is larger than 50 percent which corresponds to an absolute difference of the order of 100 W/m^2. The zonal analysis showed the largest differences are obtained in subtropical latitudes of the southern hemisphere.

2.5.3.3 Difference between the two satellite pairs NOAA-9/ERBS and NOAA-10/ERBS Figure 8 shows the relative difference between reflected solar fluxes computed from NOAA-9 and ERBS data sets and fluxes derived from NOAA-10 and ERBS data sets. The fluxes are monthly mean values computed from original ERBE data.

The two sets of data correspond to the ERB data which was available at different stages of the ERBE mission. Prior to December 1986, ERB data were provided by instruments onboard NOAA-9 and ERBS satellites and monthly fluxes were computed from this data set. After December 1986, the scanning radiometers on board NOAA-9 stopped gathering data and monitoring of the Earth's radiative field continued with ERBS and NOAA-10 observations. It was felt this was a reasonable continuity although the temporal sampling was greatly modified.

To assess the impact of the modification in the temporal distribution of the observations, one month of data is available during which the three satellites were operational simultane-

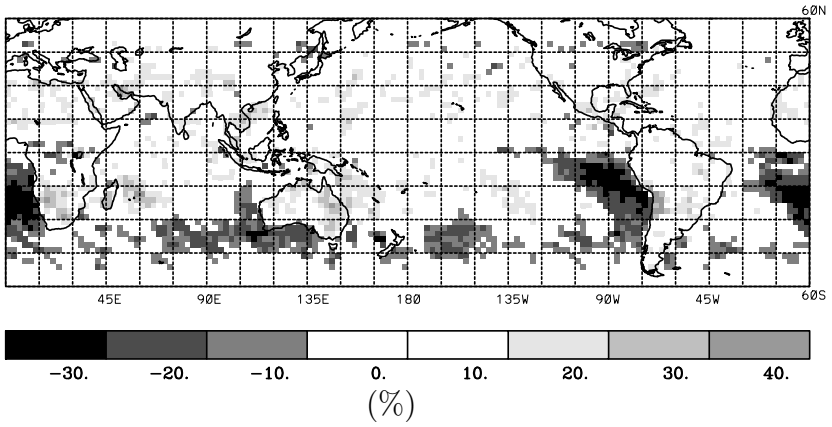

Figure 7: Relative difference between NOAA-9 and NOAA-10 based SWRE. Results obtained from ERBE original data, December 1986.

ously, December 1986. This can be done by comparing ERB products derived from two data sets, each set including the data from two satellites. This assessement is of great importance since many studies on global change, such as [10], use large time series covering several years of data to estimate interannual variations of ERB components. The change in satellite does introduce variability between the products prior to december 1986 and those after.

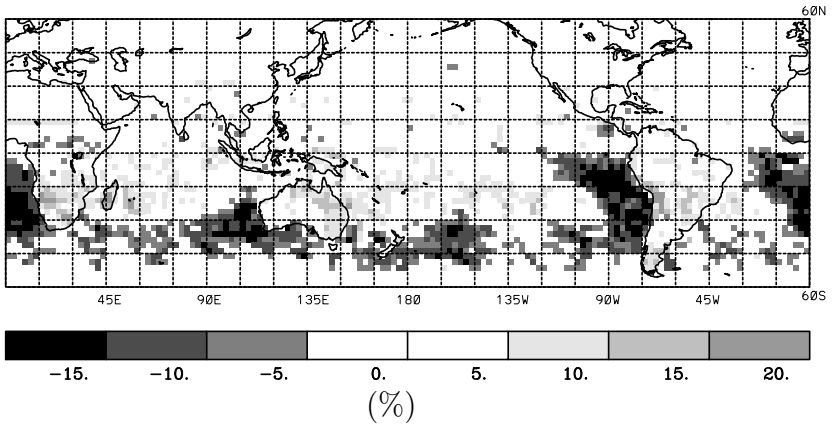

Figure 8: Relative difference between NOAA-9&ERBS and NOAA-10&ERBS based SWRE. Results obtained from ERBE original data, December 1986.

3 Improvement of the ERBE algorithm using ISCCP data

This study aims at determining to what extent ERB data sampled with a single satellite, to which correlative data is added, can produce monthly mean quantities equivalent to that obtained with multi-satellite sampled data. The ScaRaB mission operated on a single non-sun-synchronous platform slowly precessing in local time (12 hours in 104 days). In order to take into account important meteorological phenomena, correlative data could be considered to compensate for the sparse temporal coverage. Currently, geostationary satellites provide the highest temporal resolution.

3.1 ISCCP data

The International Satellite Cloud Climatology Project (ISCCP) was established in 1982 as the first project of the World Climate Research Programme (WCRP) to gather and analyse a global and uniform data base of satellite radiances dedicated to produce a new cloud climatology. Global coverage of the Earth is obtained by using a suite of geostationary platforms and polar satellites.

3.2 Spectral, spatial and temporal characteristics

The primary data used to produce cloud properties are narrowband reduced-resolution radiance measurements. Two radiometric channels are used, a visible (VIS) channel centered on 0.6 μm and an infrared (IR) channel centered on 11.0 μm. The radiances are initially obtained with a resolution of 1 to 8 km, depending on the channel and the satellite. Pixels are then sampled spatially in order to obtain a 30-km resolution, and radiances are calibrated with respect to polar-orbiter measurements. Temporal resolution of 3 h is obtained by sampling full resolution data.

Cloud analysis of ISCCP data is performed in three successive steps: cloud detection, determination of cloud parameters using a radiative transfer model and statistical analysis. Details can be found in [11].

3.3 Parameters of interest in diurnal cycles

The issue of diurnal interpolation can be approached in different fashions by using the different type of ISCCP products. In Equation 4 the scene-type fractions can be considered to be the only parameters which variations are unknown. In this case the diurnal variation of the ISCCP-derived cloud cover can be used to estimate the distribution of scene types in a region. The correspondance between ERBE and ISCCP is not straight forward. With ISCCP, the cloud classification is either binary, that is clear or cloudy, or is constructed by using nine cloud classes depending on both cloud top pressure and optical thickness. Use

of the binary classification of cloud cover to compute scene-type fractions is described in Section 3.4. Use of the nine cloud classes is described in Section 3.6.

To improve diurnal interpolation another parameter of interest certainly is the regional albedo. Instead of relying on the change of cloudiness to change the regional albedo, ISCCP measurements can be used to obtain diurnal variation of cloudiness albedo. The albedo of a scene can be inferred from parameters such as the visible reflectance or the optical thickness. Section 3.5 describes how the visible reflectance can be used to compute an albedo in the solar spectral domain.

3.4 Using monthly mean cloud cover products

The first approach is to utilize integrated cloud cover fractions to replace ERBE scene type fractions. The correspondence between the ERBE and ISCCP classification is based upon the definition of a regional albedo

$$A_{reg}(t) = A_{clr}(t)(1 - F_{ISCCP}(t)) + A_{cld}(t)F_{ISCCP}(t), \tag{5}$$

where A_{clr} is the clear sky albedo, A_{cld} is the albedo of the cloudy part and F_{ISCCP} is the ISCCP integrated cloud cover product. The very same regional albedo can be obtained from the ERBE classification

$$A_{reg}(t) = \sum_{i=1}^{4} \alpha_i[\mu(t)] f_i(t). \tag{6}$$

Correspondence is performed at times of ERBE observations t_{obs} in order to solve for $A_{cld}(t_{obs})$. The regional albedo is used in the extrapolation Equation (4) and must therefore be computed at every hour of the day using Equation (5). Diurnal variation of A_{clr} is simply given by the *clear sky* directional model. Directional variations of A_{cld} are deduced from a linear combination of the two directional models which best fit the value of A_{cld} at t_{obs}. Hourly values of F_{ISCCP} are obtained by linear interpolation between the original three hourly values. The following hypotheses are made in this algorithm:

1. Clear parts are identical in the ERBE and ISCCP classifications,
2. Directional variations of clear sky albedo in the binary classification is correctly described by the ERBE clear sky directional model,
3. Diurnal variation of cloud cover is correctly described by the ISCCP three-hourly data,
4. Diurnal variations of cloud properties, i.e. optical thickness are not taken into account.

3.4.1 Results and discussion

The algorithm described in Section 3.4 is applied to NOAA-9 and NOAA-10 data sets to produce diurnal cycles of SWRE as well as monthly mean values. The "climatological"

approach consists in using stage C2 integrated cloud cover products as correlative data. It is based upon the hypothesis that the monthly mean diurnal cycle can represent the daily diurnal cycle of cloud coverage in an unbiased manner, although random errors remain. *Duvel* [12] shows that for extensive parts of the globe the coherent diurnal variance represents a predominant fraction of the total intradiurnal variance.

3.4.1.1 Stratocumulus clouds over tropical Ocean. The algorithm is primarily applied to the stratocumulus case study of Section 2.5.1. Figure 9(a) shows five SWRE diurnal cycles of which three are original ERBE products. The two new curves, shown as dashed and long dashed thick lines, represent diurnal cycles computed from NOAA-10 and NOAA-9 data sets respectively for which correlative cloud cover information has been used.

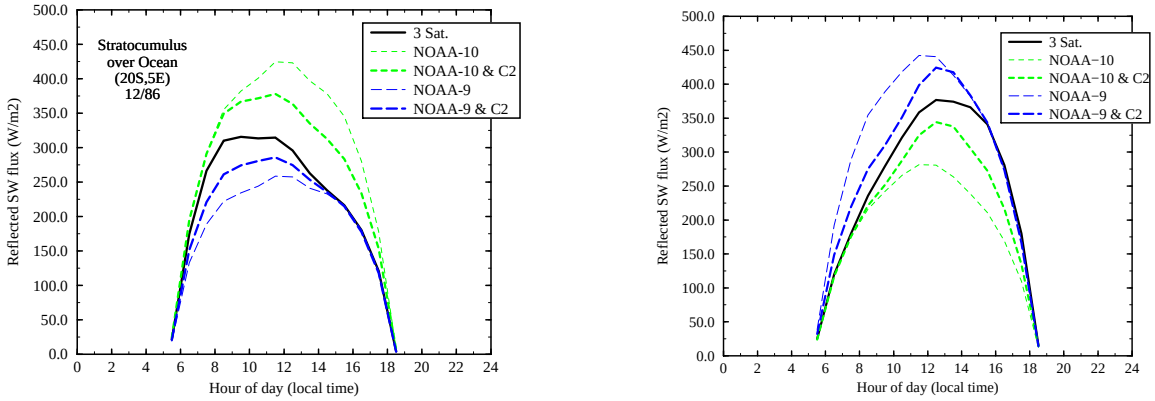

Figure 9: Monthly mean diurnal cycles of SW reflected flux based on single- or multi-satellite data. Results obtained from ERBE original data and correlative ISCCP C2 cloud cover data. December 1986; (a) Ocean, 20°S, 5°E; (b) Land, 20°S, 20°E.

As before, we consider the diurnal cycle derived from the multi- satellite data set to be the most accurate. Improvements are considered if a diurnal cycle derived from a single-satellite data set becomes closer to the multi-satellite cycle or to the other single-satellite cycle. Ideally, NOAA-9 and NOAA-10 derived cycles should be superimposed.

Figure 9(a) reveals a significant improvement for both data sets. Not only are the cycles closer to each other and to the multi- satellite curve, but also their shapes represent the realistic asymmetry between morning and afternoon. The absolute difference between NOAA-9 and NOAA-10 monthly SWRE is now about 35 W/m^2, which corresponds to a relative difference of the order of 25 percent.

3.4.1.2 Convective clouds over South-West Africa. The algorithm is then applied to a region located in Northern Namibia which is characterized by large developments of convective clouds during the day. As for the previous region, Figure 9(b) shows diurnal

cycles obtained from NOAA-9 and NOAA-10 data with and without the use of correlative ISCCP data.

The improvement provided by the use of cloud mean diurnal variability data is very significant. The diurnal cycles derived from single-satellite data sets are closer to each other and correspond better to the multi-satellite results. One can notice the strong disymetry between morning and afternoon fluxes which is due to convective development of clouds following the radiative heating of the surface.

The absolute difference between the monthly mean reflected flux derived from NOAA-9 data and NOAA-10 data has been reduced to 30 W/m^2 as opposed to 60 W/m^2 for the original data. This 50 percent improvement is very satisfactory considering the correlative data is limited to the fraction of cloud cover. In addition the variability is represented by a monthly mean product.

3.4.1.3 Global analysis. To check the validity of the algorithm, it is applied to regions in the latitude domain 50°N to 50°S. Figure 10(a) shows the relative difference between NOAA-9 and NOAA-10 derived SWRE. Radiant exitances are monthly averages computed from ERBE and correlative ISCCP C2 cloud cover data.

In Figure 10(a), negative values, shown in black and dark grey, represent regions for which the data sampled from NOAA-9 produced monthly mean fluxes smaller than NOAA-10 derived fluxes. Positive values, corresponding to NOAA-9 fluxes greater than NOAA-10 fluxes, are shown in light grey. Regions appearing in white represent either missing data or a small difference between NOAA-9 and NOAA-10 fluxes.

Figure 10(b) represent changes brought by the algorithm compared to ERBE original data. This change can be considered as the difference between Figure 7 and Figure 10(a). Regions for which the algorithm significantly improved the fluxes are shown in dark grey. If the algorithm increased the difference between NOAA-9 and NOAA-10, the region is shown in light grey. White areas represent regions where either the algorithm was not applied due to lack of ISCCP data or the algorithm did not produce a significant modification. A treshhold of 5 W/m^2 is used to determine whether the change is significant or not. This treshhold is based on the accuracy of the algorithm used to reproduce the ERBE data processing algorithm and on the accuracy of the monthly mean fluxes determined from ERBE data, which was estimated to be 5 W/m^2 in [13].

Significant improvements are found for all tropical marine stratocumulus regions. Improved monthly means are also obtained on the African and Australian continent at tropical latitudes. However, for the major part of the Northern hemisphere, this algorithm does not bring significant improvement to the data. In many of these regions, the monthly mean diurnal cycle is not very representative of the daily meteorology. This shows the limitation of using a climatological approach to improve diurnal interpolation of ERB observations.

In some cases the additional ISCCP C2 data increases somewhat the difference between NOAA-9 and NOAA-10 products. The cloud cover variation does not always represent or follow the diurnal evolution of the physical properties of the cloud. In some cases an increasing cloud cover can correspond to a decreasing optical thickness. In such a case the

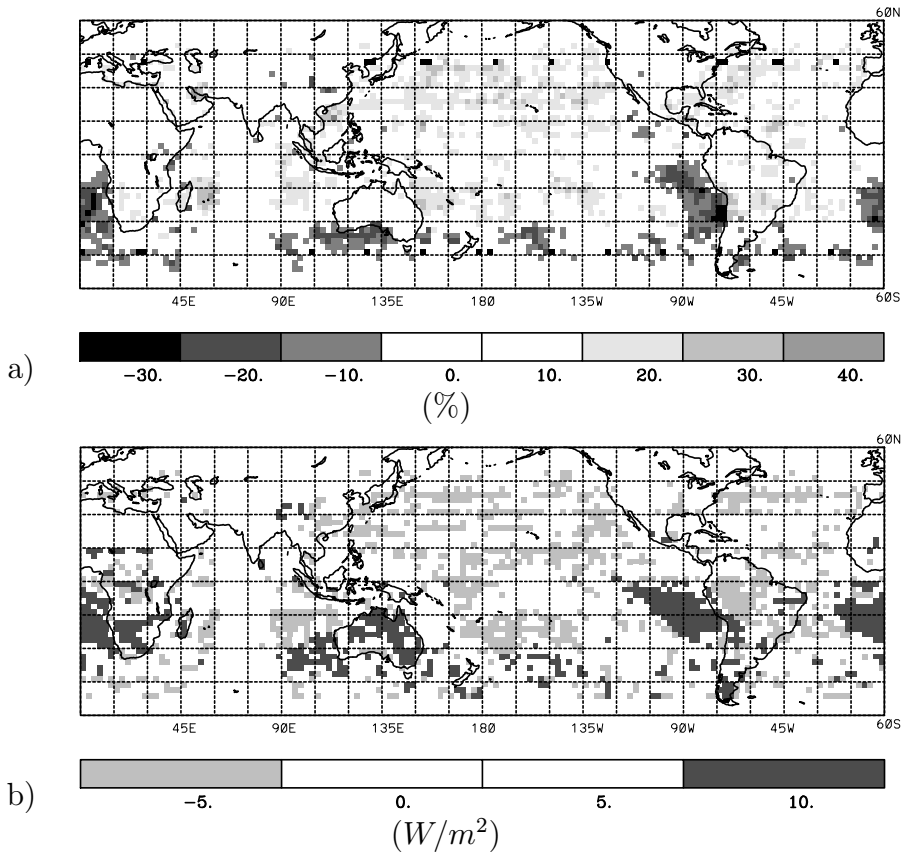

Figure 10: Difference between NOAA-9 and NOAA-10 based SWRE. Results obtained by using ERBE and correlative ISCCP C2 cloudiness data, December 1986). a) Relative difference in (%); b) Change in SWRE absolute difference (ERBE-only - ERBE-ISCCPC2).

algorithm will not take into account the important factor and the difference between the two single satellite data sets can not be corrected for. Note that no geostationary satellite information is available in the longitude domain 60°E to 75°E due to missing INSAT data.

3.5 Using daily ISCCP cloud parameters

This last point is very important since, for example in regions where important convective activity takes place, the optical thickness of the cloudy atmosphere can vary significantly from sunrise to sunset.

In addition to cloud cover products, stage C1 data provide the average radiance measurements in the visible and infrared spectral domain which were used to determine the amount of cloud cover and other parameters such as the optical thickness. The average radiances are provided separately for clear and cloudy pixels. In fact the parameter called visible radiance, *VIS RAD*, is the measured visible radiance, L^{VIS}_{mes}, expressed with respect to E^{VIS}_0, the

solar constant weighted by the instrument spectral response and sorrected for the Sun-Earth distance,

$$L^{VIS}(\theta_0, \theta, \phi) = \frac{L^{VIS}_{mes}(\theta_0, \theta, \phi)}{E^{VIS}_0}. \tag{7}$$

This radiance can be considered as a *normalized radiance*, it is dimensionless. This radiance gives an indication of the opacity of the cloud. A bidirectional reflectance can be derived from the normalised radiance,

$$R^{VIS}(\theta_0, \theta, \phi) = \frac{L^{VIS}(\theta_0, \theta, \phi)}{cos\theta_0}, \tag{8}$$

where the solar zenith angle θ_0 is taken to be value which spatially and temporally corresponds to the pixel of interest. So the value which is obtained from the parameter called *VIS RAD* is in fact a bidirectional reflectance under overhead-sun conditions. No angular correction is applied to take into account the changes in measuring geometry as a function of the relative location of satellite and the observed geographical point. Motivation for this can be found in the ISCCP cloud data documentation [14].

3.5.1 ISCCP-radiance to ERBE-albedo conversions

The visible radiances of cloudy pixels can be converted into SW albedos by taking into account bidirectional and directional effects. In a first step ERBE regional albedos (ERBE type S9 product) are compared to cloud-cover normalized radiances issued from ISCCP C1 data. The comparison is performed on measurements which are quasi simultaneous and co-located with identical scene-type identification. The difference between the cosines of the solar zenith angles can not be greater than 0.1 and measurements ca not be more than one hour and a half apart. To get the best possible match, only cloudy pixels are considered within a 2.5° region, and the ERBE albedo is computed as the weighted sum of the albedos of the three cloudy scene types.

Figure 11 shows ERBE regional albedos as a function of normalized radiances for eight different intervals of solar zenith angle. The underlying surface is ocean in Figure 11(a) and land in Figure 11(b). The correlation between the two variables greatly depends upon the solar zenith angle. For a given ISCCP radiance, if the solar angle increases, the ERBE albedo will increase as described by the ERBE directional models.

Figure 12 shows the same ERBE albedos as a function of ISCCP visible radiances, taking into account the zenith angle of the incoming solar radiation. The angular dependence is greatly reduced. All the curves are close together and have approximatively the same slope. The alignement is not perfect because in the ISCCP data inversion, the anisotropy of the scene is not accounted for in the visible radiance parameter. The difference between the curve increases with increasing θ_0 angle, which corresponds to the known behavior of directional angular models. The difference is greater for low albedos because they correspond to clear or partly cloudy scenes. According to directional angular models, the anisotropy of such scenes is important. The difference becomes smaller as the albedo increases since large

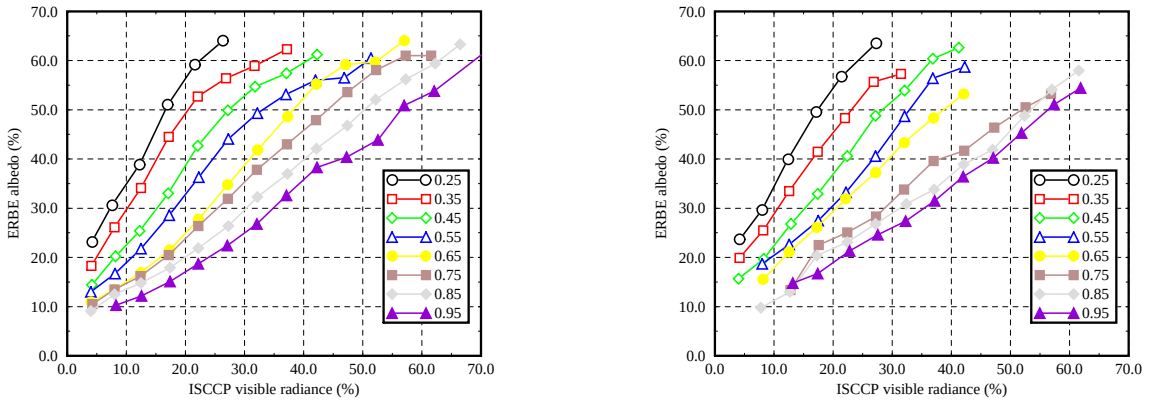

Figure 11: ERBE regional albedo as a function of ISCCP normalized visible cloud radiance. Each curve corresponds to a particular solar zenith angle. Underlying surface is (a) ocean and (b) land.

albedos usually correspond to mostly cloudy or overcast scenes which are highly isotropic. Furthemore, a significant difference is observed between ocean and land surfaces. The scene anisotropy is significantly less for land surfaces than for oceans. Thus, for land surfaces, the difference between ERBE albedos and ISCCP reflectance is less sensitive to cloud cover.

In spite of possible bias in the regression, angular correlations are established to compute ERBE shortwave albedos for any given solar zenith angle from a normalized visible radiance. These angular correlations are similar to ERBE directional angular models in that they give the variation of shortwave albedos as a function of solar zenith angle variations. The difference is that the various cloud conditions are represented by seven intervals of ISCCP normalized radiances instead of the four ERBE scene types.

Figure 13 shows the relation between the ISCCP normalized radiance and the ERBE albedo for overhead sun conditions ($0.9 < \cos\theta_0 < 1.0$). This relation can be written in the form of a third-order polynomial

$$A_{neb}(\theta_0 = 0) = C_0 + C_1 L^{VIS}(\theta_0 = 0, \theta, \phi) + C_2 L^{VIS}(\theta_0 = 0, \theta, \phi)^2 + C_3 L^{VIS}(\theta_0 = 0, \theta, \phi)^3 , \quad (9)$$

where L^{VIS} is the radiance defined in Equation 7. Coefficients C_i are identical for ocean and land underlying surfaces.

C_0	C_1	C_2	C_3
8.20560	0.12297	0.01950	-0.00015

Once the overhead sun ERBE albedo has been computed the albedo corresponding to the actual illumination conditions must be computed. For this, an angular variation model

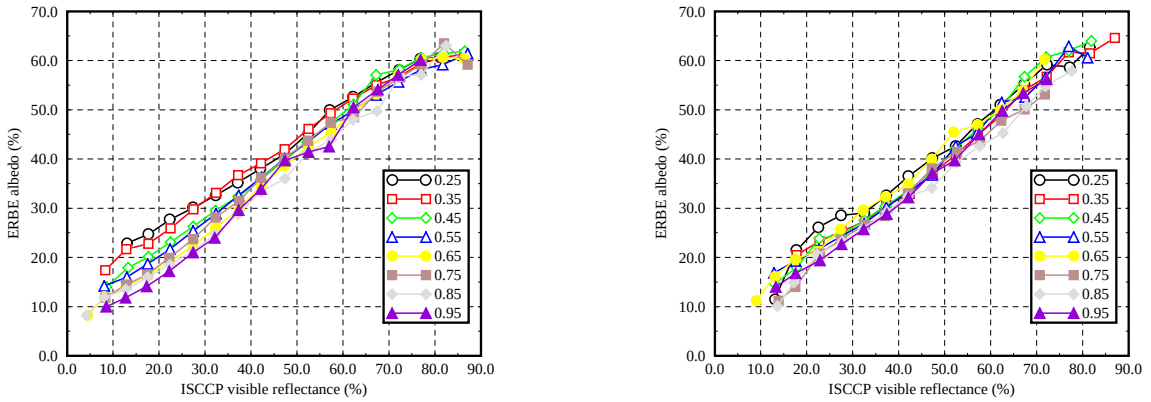

Figure 12: ERBE regional albedo as a function of ISCCP visible cloud reflectance. Each curve corresponds to a particular solar zenith angle. Underlying surface is (a) ocean and (b) land.

of the ERBE albedo with solar zenith angle has been established for each of seven intervals of normalized ISCCP radiance. The seven intervals represent seven conditions of cloud cover opacity. Figure 3.5.1 shows the angular models for ocean and land surface. The models are defined as a second order polynomial in θ_0 in which the zero order term is a function of $A_{neb}(\theta_0 = 0)$

$$A_{neb}(\theta_0) = 0.01 C_0 A_{neb}(\theta_0 = 0) + C_1(0.01\theta_0) + C_2(0.01\theta_0)^2 \ . \tag{10}$$

The C_i coefficients used for ocean and land surface are given in Table 1.

Table 1: Coefficients of Equation 10 defining the angular variation of the ERBE albedo for various intervals of cloud cover opacity (ISCCP normalized radiance).

Normalized Radiance (%)	Coefficients of Equation 10					
	Ocean			Land		
	C_0	C_1	C_2	C_0	C_1	C_2
0 - 10	1.56890	-0.41628	0.71862	1.60880	-0.49296	0.67366
10 - 20	1.50950	-0.63933	1.14780	1.42910	-0.42102	0.90134
20 - 30	1.27430	-0.52742	1.18980	1.29510	-0.51254	1.29180
30 - 40	1.0073	-0.18925	0.90791	0.78109	0.22466	0.44569
40 - 50	0.87204	0.09930	0.56512	0.77097	0.39485	0.15933
50 - 60	0.92820	0.07545	0.46763	0.99874	0.08078	0.44418
60 - 70	0.98342	0.00012	0.40179	0.97122	0.14874	0.17136

The conversion of ISCCP radiances into ERBE albedos is not sufficient to establish a

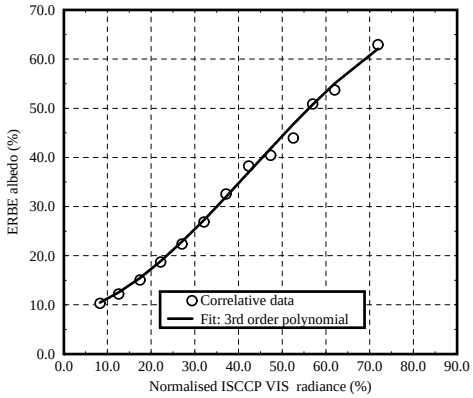

Figure 13: ERBE regional albedo as a function of ISCCP visible cloud radiance for zenithal solar conditions ($0.9 \leq \cos\theta_0 \leq 1.0$).

complete diurnal cycle of SW reflected fluxes. For the ERBE algorithm one value per hour box is required. Completion of the diurnal cycle where ISCCP data are not available is an issue for which it is difficult to find one general solution.

3.5.2 Completion of the diurnal cycle of the albedo

Interpolations and extrapolations must be treated separately. Interpolations are performed for hour boxes included between the first and last ISCCp measurement. For such hour boxes, the normalized radiance is computed by applying a linear interpolation between two successive ISCCP measurements. After the solar zenith angle has been determined, Equations 9 and 10 can be used to compute the albedo of the regional cloud cover. Extrapolations are used for hour boxes between sunrise and the first ISCCp measurement and between the last ISCCP measurement and sunset.

3.5.3 Results and discussion

This algorithm is applied to NOAA-9 and NOAA-10 data to compute diurnal cycles of SW reflected fluxes as well as monthly mean values.

3.5.3.1 Stratocumulus clouds over tropical Pacific. The algorithm is applied to the stratocumulus region described in Section 2.5.1. Figure 15(a) shows five diurnal cycles of which three are derived from original ERBE data and two are new. The new curves, shown as dashed and long-dashed thick lines, represent diurnal cycles computed from NOAA-10 and NOAA-9 data sets respectively for which correlative cloud cover and cloud albedo information has been used.

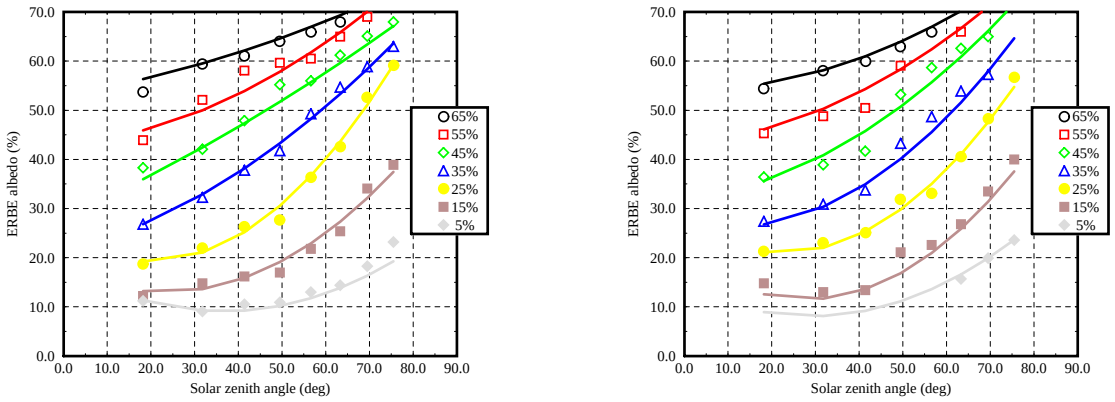

Figure 14: Directional modele of the ERBE regional albedo as a function of the solar zenith angle for various normalized cloud radiances. Underlying surface is (a) *ocean* and (b)*land*.

As before, we consider the diurnal cycle derived from the multi-satellite data set to be the most accurate. Improvements are considered if a diurnal cycle derived from a single-satellite data set becomes closer to the multi-satellite cycle or to the other single-satellite cycle. Ideally, NOAA-9 and NOAA-10 derived cycles should be superimposed.

Figure 15(a) reveals a significant improvement for both data sets if compared to the original ERBE data. Thes improvements are greater than the ones shown in Figure 9(a). The two single-satellite cycles are now very close to each other and close to the multi-satellite cycle. The original single-satellite cycles were symetrical with respect to solar noon because they were based on a single measurement and considered the cloud cover to remain constant through out the day. Use of cloud-cover and normalized-radiance variations allows the asymetry of the regional albedo between morning and afternoon to be taken into account. The shapes of the two single-satellite cycles are now very similar to the multi-satellite curve.

The absolute difference between NOAA-9 and NOAA-10 monthly SW reflected flux is now about 15 W/m^2 instead of 70 W/m^2 for the original ERBE data. This absolute difference corresponds to a relative difference of 10 percent as opposed to 50 percent originally.

3.5.3.2 Convective clouds over South-West Africa. Figure 15(b) shows diurnal cycles of reflected solar fluxes derived from NOAA-9 and NOAA-10 measurements with and without correlative cloudiness data. The absolute difference between the reflected solar fluxes derived from NOAA-9 and NOAA-10 is less than 5 W/m^2. This result must be interpreted with caution eventhough the single-satellite monthly mean fluxes are within 5 W/m^2 of the multi-satellite result.

On average, four ISCCP measurements are obtained over this region during the day-light hours, the first measurement being close to sunrise and the last in the late afternoon. The relative value of the first measurement with respect to the other measurements the same

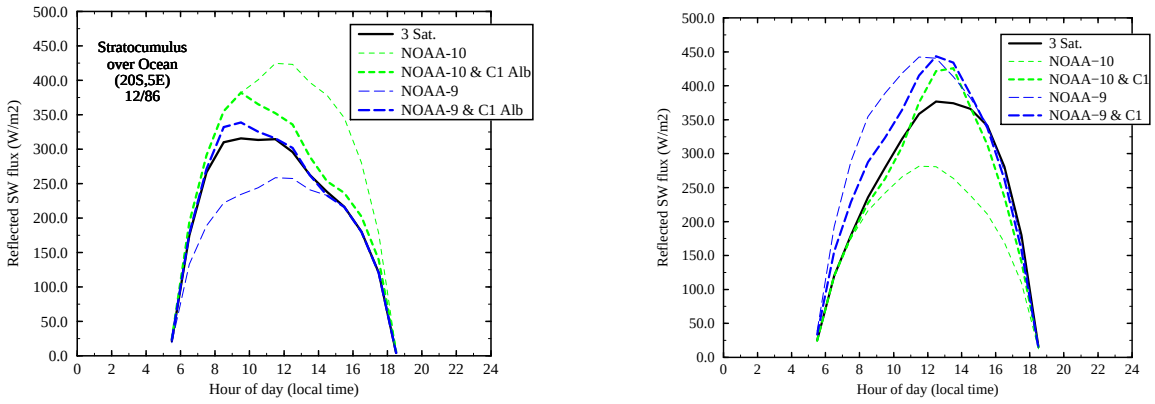

a) b)

Figure 15: Monthly mean diurnal cycles of SW reflected flux based on single- or multi-satellite data. Results obtained from ERBE original data and correlative ISCCP C1 cloud cover and normalized radiance data. December 1986; (a) Ocean, 20°S, 5°E; (b) Land, 20°S, 20°E.

day has a very significant effect on the diurnal extrapolation performed from a NOAA-10 measurement, both in terms of normalized radiance and cloud cover. This effect is revealed in Figure 15(b). The diurnal cycle of solar reflected flux derived from NOAA-10 data is modified in a much greater fashion than is the cycle derived from NOAA-9 data. If we assume that the uncertainty associated with a very early morning measurement is greater than the uncertainty at any other time because of the very low solar elevation, correction of NOAA-10 diurnal cycles will not be as reliable as the correction of NOAA-9 derived products. This effect varies of course from one region to the next since the result depends on a combined effect of the time of measurement and meteorology.

3.5.3.3 Global study. To check the validity of the algorithm, it is applied to all longitudes, between latitudes 50°N and 50°S. Figure 16 shows the relative difference between NOAA-9 and NOAA-10 derived SWRE. Exitances are monthly averages computed from ERBE and correlative ISCCP stage C1 data.

Very significant improvements are found for all tropical marine stratocumulus regions. Note in particular marine regions west of the South American coast in the latitude interval 15°S to 45°S. However, in some cases, the correlative ISCCP C1 data increases significantly the difference between NOAA-9 and NOAA-10 products.

In the equatorial Pacific ocean west of Indonesia significant negative and positive differences are observed next to each other. Studying the temporal sampling of ISCCP data reveals that this area corresponds to a geostationary satellite limit. The diurnal sampling of regions east of this limit, appearing with negative differences, is shifted three hours earlier than that of the western regions. We believe this sampling introduces biased diurnal cycles

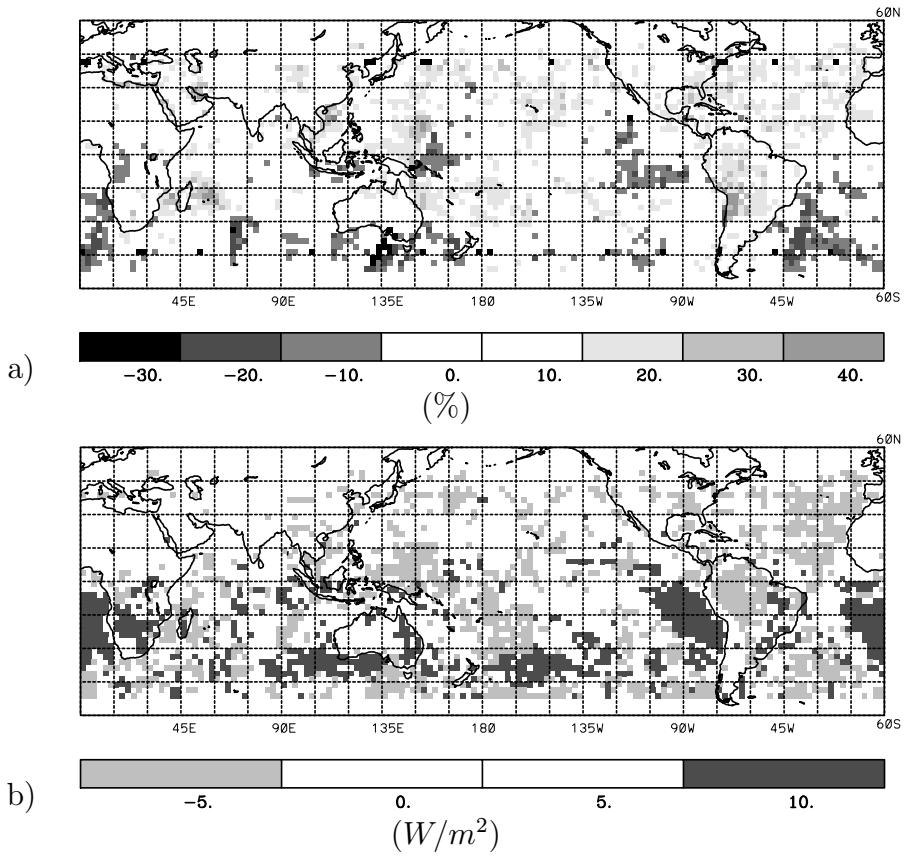

Figure 16: Difference between NOAA-9 and NOAA-10 based SWRE. Results obtained by using ERBE and correlative ISCCP C1 cloudiness and radiance data, December 1986. a) Relative difference in (%); b) Change in SWRE absolute difference (ERBE-only - ERBE-ISCCPC1).

of cloud properties which must be studied with care before utilizing them to improve diurnal interpolation of ERB observations.

3.6 Using the ISCCP cloud classification

The ISCCP cloud classification allows both the cloud optical properties and the cloud cover extent to be taken into account. The cloud classes are defined in terms of cloud top pressure and cloud optical thickness, as is shown in Table 2. There are three levels of altitude, low, medium and high and three intervals of optical thickness, thin, medium and opaque, which discriminate the clouds in nine classes.

As was described in Section 3.5, it is of great importance to characterize the diurnal variation of the regional albedo. This can be done by defining directional models which represent the angular dependance of the albedo to variations of the solar zenith angle, for

Table 2: Radiometric definition of cloud types in the ISCCP data base. The six highest cloud types can be liquid or ice clouds depending on if the temperature at the top of the cloud is above or below 260 K.

Altitude	Pressure (mBar)	Cloud types		
High	50 - 440	Cirrus	Cirrostratus	Deep Convection
Middle	440 - 680	Altocumulus	Altostratus	Nimbostratus
Low	680 - 1000	Cumulus	Stratocumulus	Stratus
Optical thickness		0 - 3.6	3.6 - 23	23 - 379

each type of cloud. The angular models are determined from spatially and temporally co-localized ERBE and ISCCP measurements. Co-localization is considered when for a given 2.5° region, the cosine of the solar zenith angles of the two meaurements are within 0.1 of each other and the difference in time of measurement is less than an hour and a half. The albedo of the cloud cover defined by ERBE is then affected to the major cloud type defined by ISCCP.

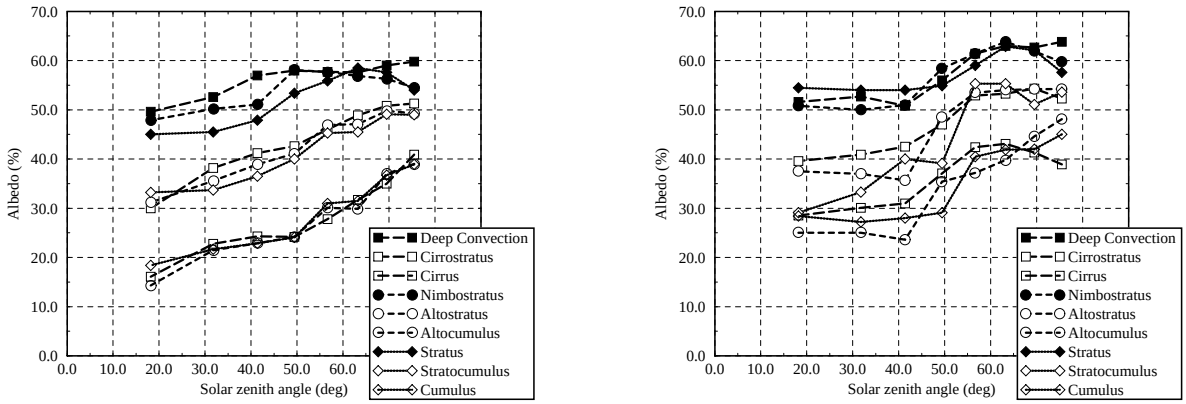

a) b)

Figure 17: Angular directional model of the ERBE regional albedo as a function of the solar zenith angle for various ISCCP cloud types. The geographical type of the underlying surface is *ocean* (a) and *land* (b).

Figure 17 shows the angular models as a function of cloud types for underlying surfaces ocean and land. The figure clearly shows that there are three distinctive cloud groups. Deep convection clouds, nimbostratus and stratus clouds, respectively high middle and low altitude clouds are opaque clouds. The angular variations of the albedo associated with these three types of clouds are similar to that associated with overcast conditions defined by the ERBE scene identification algorithm. Due to atmospheric absorption and scattering, the high altitude clouds are more opaque than the middle altitude clouds which in turn are

more opaque than the low altitude clouds.

Similarly, cirrostratus, altostratus and stratocumulus clouds are gathered as medium optical thickness clouds. For these cloud type the angular variation of the albedo is similar to the mostly cloudy class of the ERBE classification. The actual albedo values fall between overcast and mostly-cloudy types of ERBE albedos.

Finally, the three thin cloud types, cirrus, altocumulus and cumulus, behave similarly to clouds in the partly-cloudy or mostly-cloudy ERBE types.

The correspondence between the ISCCP and ERBE cloud classification is a good indicator that the latter is not exclusively based on the fraction of cloud cover, but also, in an implicit way, on the optical properties of the clouds.

The algorithm using the ISCCP cloud types is nearly identical to the original ERBE interpolation and extrapolation algorithm described in [6]. The flux $M_{SW}(t')$ can be computed from a given observation $M_{SW}(t_{obs})$ as

$$M_{SW}(t') = \frac{\mu(t')}{\mu(t_{obs})} \frac{\sum_{i=1}^{9} \alpha_i[\mu(t')] f_i(t')}{\sum_{i=1}^{9} \alpha_i[\mu(t_{obs})] f_i(t_{obs})} M_{SW}(t_{obs}), \tag{11}$$

where $f_i(t)$ is the cloud fraction of ISCCP cloud type i and $\alpha_i[\mu(t)]$ the corresponding albedo.

3.6.1 Results and discussion

The algorithm is applied to NOAA-9 and NOAA-10 data to compute diurnal cycles of SW reflected fluxes as well as monthly mean values.

3.6.1.1 Stratocumulus clouds over tropical Pacific. The algorithm is applied to the stratocumulus region described in Section 2.5.1. Figure 18(a) shows five diurnal cycles of which three are derived from original ERBE data and two are new. The new curves, shown as dashed and long-dashed thick lines, represent diurnal cycles computed from NOAA-10 and NOAA-9 data sets respectively for which correlative cloud cover and cloud albedo information has been used.

As before, we consider the diurnal cycle derived from the multi-satellite data set to be the most accurate. Improvements are considered if a diurnal cycle derived from a single-satellite data set becomes closer to the multi-satellite cycle or to the other single-satellite cycle. Ideally, NOAA-9 and NOAA-10 derived cycles should be superimposed.

Figure 18(a) reveals significant improvements in the diurnal cycles computed using the ISCCP cloud classification data compared to ERBE original products. One can note the strong asymetry between morning and afternoon fluxes. The maximum reflected solar flux is obtained around 10:30 am which corresponds to a time for which the incoming solar flux is already very large and the cloud cover has not yet dissipated. After 10:30 am the increase in incoming solar radiation is compensated by the decrease in cloudiness and cloud optical

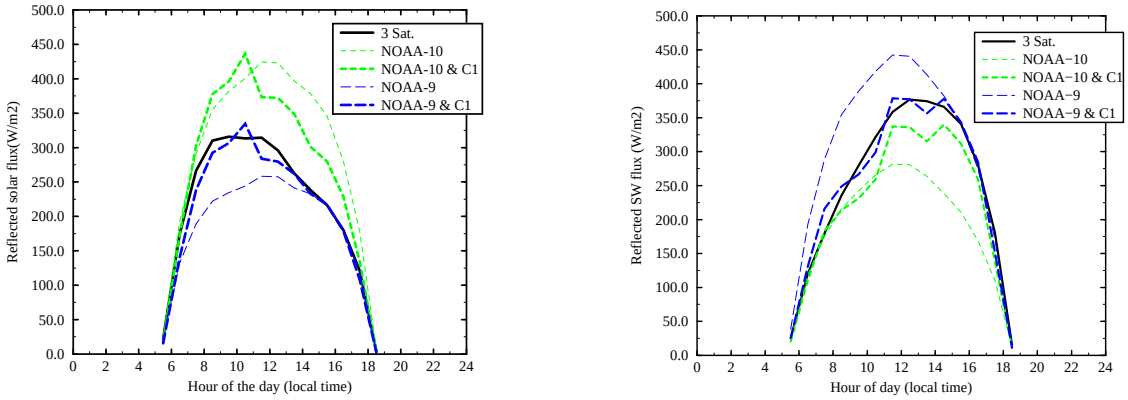

a) b)

Figure 18: Monthly mean diurnal cycles of SW reflected flux based on single- or multi-satellite data. Results obtained from ERBE original data and correlative ISCCP C1 cloud classification data. December 1986; (a) Ocean, 20°S, 5°E; (b) Land, 20°S, 20°E.

thickness such that the reflected flux starts to decrease. It is very clear that the diurnal cycle of cloudiness has a very determinant effect on the amount of radiation which will be available to heat up the Earth and atmosphere.

The absolute difference between the monthly mean derived from NOAA-9 and that derived from NOAA-10 is now close to 15 W/m^2 as opposed to 70 W/m^2 as given by the original ERBE data. This difference corresponds to a relative difference in the order of 10 percent. For this particular region, the cloud classification data does not allow as good a correction as does the ISCCP radiance data. Indeed, this method can be considered to average out the cloud information since the radiance data are essentially interpreted in terms of a limited number cloud types.

3.6.1.2 Convective clouds over South-West Africa. For this region aswell, the ISCCP cloud classification provides the necessary information on the diurnal variations of the properties of the cloud cover. The diurnal cycles, as explained for the stratocumulus region case study, are shown in Figure 18(b). The disymetry between morning and afternoon is well represented which confirms that the angular models derived for land regions are satisfactory. The change in optical properties of the cloud cover between morning and afternoon is characterized in the ISCCP data as a change from cumulus clouds in the morning to cumulonimbus clouds in the afternoon. The strong vertical development of clouds is due to the surface heating which increases the lapse rate leading to unstable rising air. This pattern is repeated every day with little interdiurnal variations.

It is interesting to notice, by comparing Figure 18(b) to Figure 9(b), that the use of the cloud classification associated with angular models brings considerable improvements in the correction of single -satellite products compared to the use of the total cloud fraction. The

cloud classification allows variations in the optical thickness to be accounted for which is an important factor in the diurnal variations of the albedo.

NOAA-9 data associated with ISCCP data produce a particularly good diurnal cycle, superimposed on the diurnal cycle derived from the multi-satellite data set. The NOAA-9 derived monthly mean is almost exactly that obtained from the three-satellite data set. The difference in monthly mean reflected shortwave flux between NOAA-9 and NOAA-10 is 15 W/m^2, which represents a 75 percent decrease with respect to the difference in the original data.

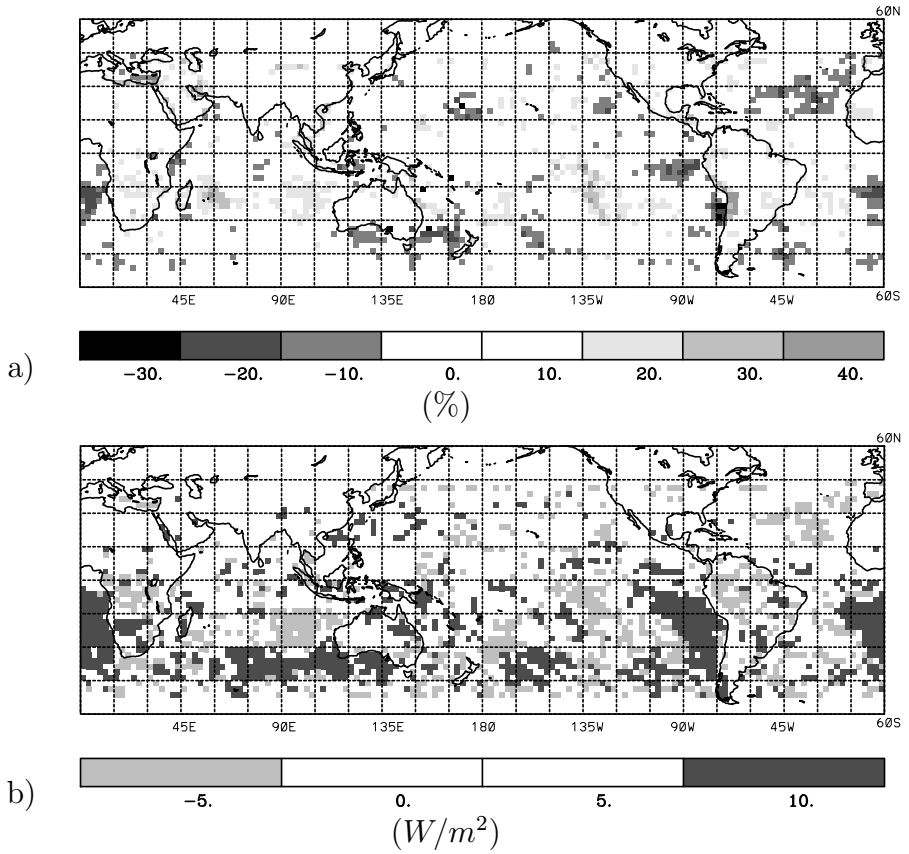

Figure 19: Difference between NOAA-9 and NOAA-10 based SWRE. Results obtained by using ERBE and correlative ISCCP C1 cloud classification data, December 1986. a) Relative difference in (%); b) Change in SWRE absolute difference (ERBE-only - ERBE-ISCCPC1).

3.6.1.3 Global study. To validate the algorithm, we apply it to all regions between 50°N and 50°S. Figure 19(a) shows the relative difference between SW reflected fluxes derived from NOAA-9 and NOAA-10 data. Fluxes are monthly mean computed from ERBE data and correlative cloudiness data issued from the ISCCP C1 cloud classification products. Figure 19(b) represents deviation from ERBE original data after the algorithm is applied.

This change can be considered as the difference between Figure 7 and Figure 19(a). For details about the color pattern, refer to Section 3.4.1.3.

Studying Figure 19 reveals significant improvements in the major part of the southern hemisphere. As before, the tropical ocean regions covered by stratocumulus clouds show great improvements. The detection of low level clouds over oceans works very well and the temporal coverage of meteorological phenomena in the southern hemisphere is very satisfactory.

The areas where the algorithm is not successfull are the northern Atlantic, the southern Pacific and the eastern Indian ocean. Part of the difficulty can be explained by cloud identification problems for high altitude ice crystal clouds. A radiative transfer model in the shortwave spectral domain is used to compute visible radiances as a function of the measuring geometry, the illumination conditions, the surface reflectance, the cloud optical thickness and the cloud-top pressure. There results a conversion table which is inverted to be used for cloud characterization. Thus, given a visible radiance corrected for the Earth-Sun distance and ozone absorption, given the angles of observation and illumination, and given the surface reflectance and the cloud-top pressure, the table can be used to obtain the cloud optical thickness. This identification depends on the definition of clouds in the radiative transfer model. Scattering within clouds is defined by the Mie theory applied to spherical droplets. This representation is not adapted to high altitude clouds which are generally made of ice crystals.

3.6.1.3.1 Normalized radiance and optical thickness. Figure 20 shows three maps of optical thickness corresponding to three successive ISCCP measurements. Figure 21 represents the corresponding three maps of cloud reflectance. In comparing Figure 20 to Figure 21, one can see that the major patterns of strong optical thickness correspond to regions of strong reflectance. Though, in Figure 20(b) there is a region at the far East of the map, about 5° wide, for which the values of optical thickness are stronger than for the neighboring regions. In Figure 21(b) there is a corresponding, although much weaker, pattern. This indicate the possibility of a bias in the radiative transfer model used to compute the optical thickness, because the area can be associated with very low solar elevations. This can be understood by studying the preceeding and following maps.

Regions close to the equator on the 00 GMT map were observed at about 4:30 pm local time which is close to sunset at this time of the year. On the 21 GMT map the day before, the local time in this area is 1:30 pm. On this map, Figure 20(a), the pattern of strong optical thickness along the day-night limit on the 00 GMT map does not appear. On the other hand, the other patterns of strong optical thickness are already present. This shows an artefact of the ISCCP visible transfer model for the inversion of radiances into optical thickness.

This error is also found in the monthly mean C2 data. Indeed, in the curse of a month, the day-night limit moves only a few degrees in longitude and hence the regions observed under extreme illumination conditions are always the same. Therefore, the monthly mean optical thickness has the same bias as the instantaneous values.

This bias is significant and we can assume that for regions oberved under extreme illu-

mination conditions, clouds will be considered to be more opaque than they really are.

3.6.1.3.2 Bias in the angular model. The angular models based on ISCCP cloud types and thus on cloud optical thickness show the bias described in the previous paragraph. For large solar zenith angles, that is greater than 65°, the optical thickness values seem to be artificially high. The direct implication is that the cloud optical thickness will be overestimated. This can be observed in Figure 17. The curves for medium and opaque clouds tend to reach a plateau around 60° and the albedo even decreases beyond 65°. For stratus and nimbostratus clouds the albedo value at 70° corresponds to that of clouds of medium opacity, whereas they are defined as opaque clouds. The clouds are identified as opaque because of the artificial increase in optical thickness for these solar angles, but the ERBE albedo remains that of a scene which can be classified as mostly cloudy rather than overcast.

Thus while the general shape of the angular models is satisfactory, a significant bias is found for solar angles larger than 60°. The impact of this bias should not be underestimated because of the relative importance of low fluxes associated with these solar angles. On the contrary, to compute diurnal cycles from measurements made early in the morning, for instance with NOAA-10, or late in the afternoon, it is very important to have a good accuracy on the albedo value because the entire extrapolation and thus the large flux values close to the solar noon, depend on the value of this albedo.

4 Conclusions

Due to sparse temporal sampling, polar orbiting satellites can not resolve the complete diurnal cycle of SWRE. Over extensive parts of the globe, significant biases can be propagated to the monthly means when the diurnal cycles of cloud cover and cloud properties are not correctly sampled. Data sets obtained from NOAA-9 and NOAA-10 can produce monthly mean SWRE which differ by more than 50 percent.

Using correlative cloud cover information issued from ISCCP stage C2 data can improve significantly the time averaging algorithm, in particular for regions where clouds have a pronounced diurnal cycle. Further improvement can be obtained by using daily information about cloud cover variability and including cloud optical thickness data. Two products issued from the ISCCP stage C1 data can be used, the normalized cloud radiance or the cloud classification data. To use either parameter, angular dependance models must be developed to represent the variation of the cloud albedo with the solar zenith angle for given conditions corresponding to different values of the ISCCP parameter.

Figure 22(a) shows mean values of the flux difference between NOAA-9 and NOAA-10 as a function of latitude for ocean regions. Positive values correspond to NOAA-9 fluxes larger than NOAA-10 fluxes. The curve representing the original ERBE data shows a positive bias in the northern hemisphere and a negative one in the southern hemisphere. In the southern hemisphere, the bias is nearly zero in the subtropics and reaches a maximum in the middle

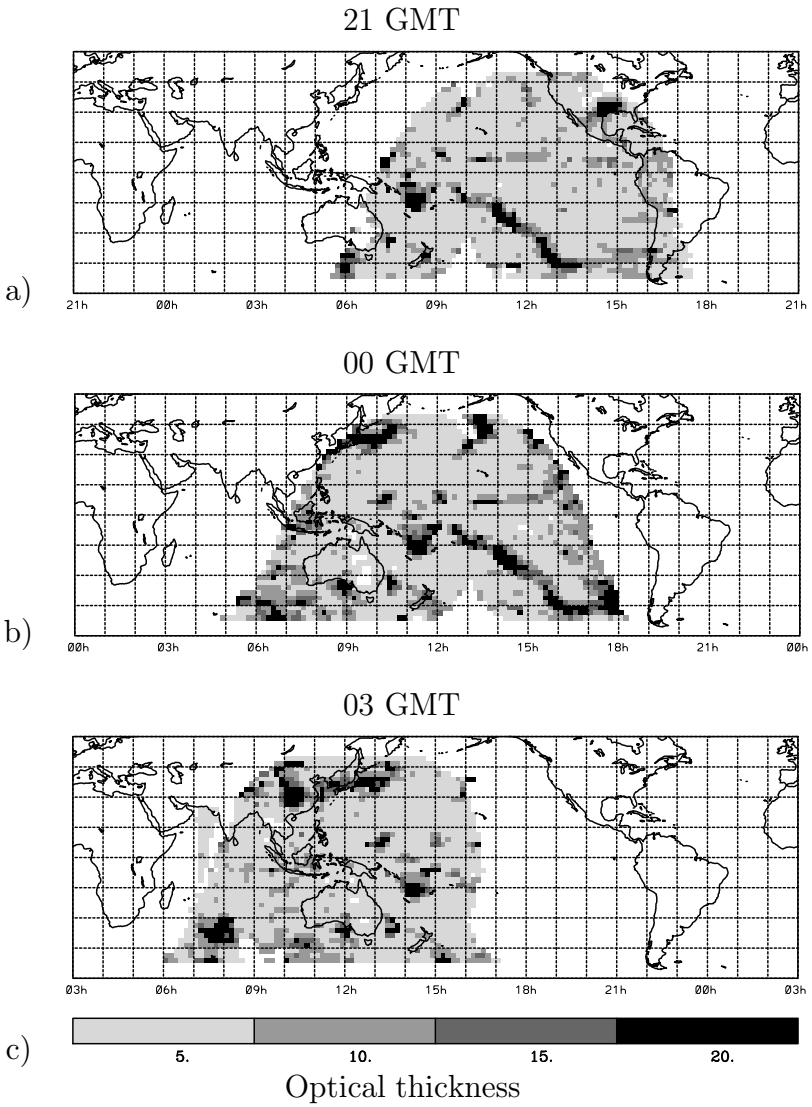

Figure 20: Cloud optical thickness, ISCCP C1 data. a) December 14, 1986 at 21GMT; b) December 15, 1986 at 00GMT; c) December 15, 1986 at 03GMT.

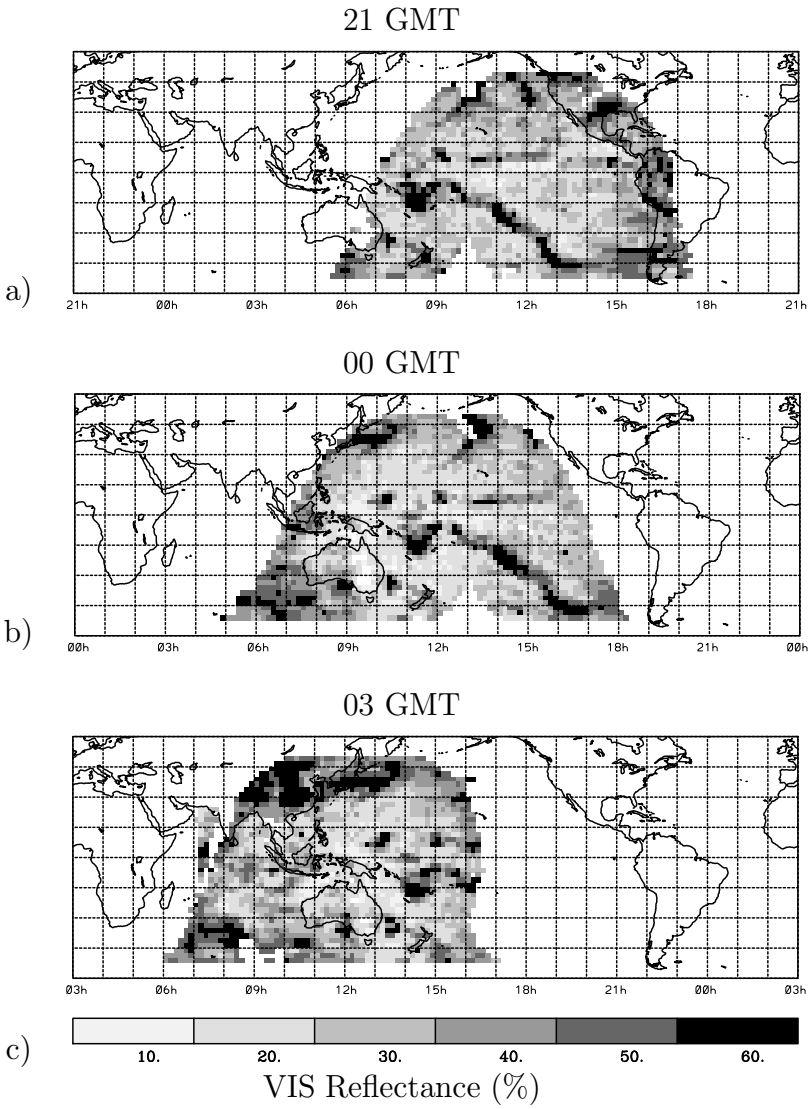

Figure 21: Cloud VIS reflectance, ISCCP C1 data. a)December 14, 1986 at 21GMT, b)December 15, 1986 at 00GMT, c)December 15, 1986 at 03GMT.

latitudes.

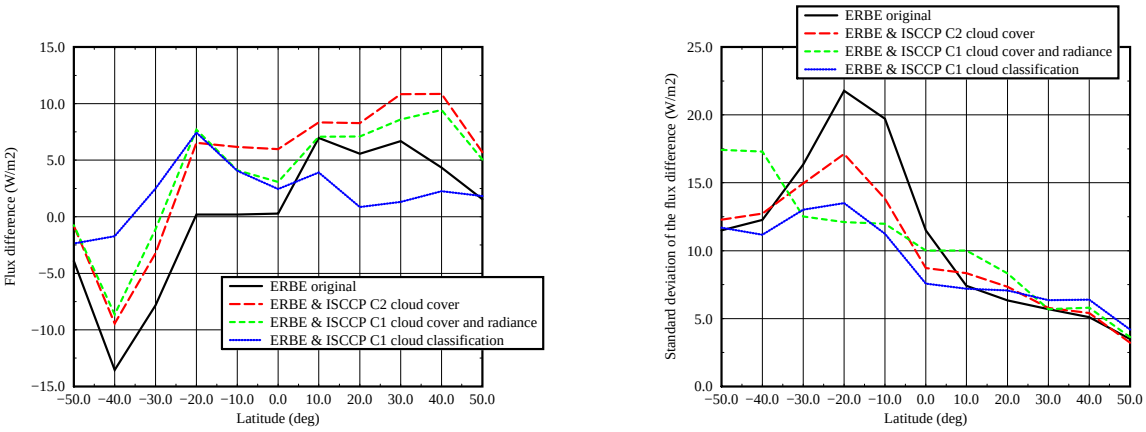

a) b)

Figure 22: (a) Mean and (b) standard deviation pe latitude of the difference between NOAA-9 and NOAA-10 derived monthly mean reflected solar fluxes for the various algorithmss presented in this paper. December 1986, ocean surfaces..

Of the three methods presented in this paper, the one which uses the ISCCP cloud classification associated with angular models seems to be the most suitable. For most latitudes, this method produces a bias which is significantly lower than the original one. The high bias around 20°S, which is common to the three methods, is due to the efficient correction for ocean regions covered by low stratiform clouds combined with less successful corrections at other longitudes. As explained before, the ISCCP data are not as suitable for detection of high altitude clouds.

Figure 22(b) shows the standard deviation around the mean of Figure 22(a). On average over all the latitudes, the use of ISCCP cloud classification is the most efficient method to take into account the diurnal variability of cloudiness. It is interesting to note that the general trend of the standard deviation is to increase from 50°N to 50°S. This is due to the distribution of the insolation on the Earth at that time of the year. For the original ERBE data the maximum values are found at the tropics of the southern hemisphere which corresponds to maximum insolation in december. This pattern will not be modified significantly by plotting relative values instead of absolute ones. The correlation with the distribution of insolation is related to the correlation between amount of incident solar radiation and meteorological activity.

Improved results from our algorithm which uses the ISCCP cloud classification data can be expected in the future, after the ISCCP data has been reprocessed with a new radiative transfer model with improved optical thickness computations. Part of the improvement can be associated with the distinction between ice and liquid water clouds according to their altitude. Details about the new cloud data sets were just released in [15].

5 Acknowledgement

The work on which this paper is based was supported in part by the Centre National d'Etudes Spatiales and the European Space Agency. We are indebted to our colleagues at LMD, in particular J.-P. Duvel and M. Viollier, for many useful discussions regarding scientific and technical issues, P. Raberanto and D. Thomas, for assistance with data processing. We also thank W. Rossow for helpful discussions regarding ISCCP.

References

[1] Bruce A. Wielicki and Richard N. Green. Cloud identification for ERBE radiative flux retrieval. *Journal of Applied Meteorology*, 28:1133–1146, November 1989.

[2] B. R. Barkstrom. The earth radiation budget experiment (erbe). *Bulletin of American Meteorological Society*, 65:1170–1185, 1984.

[3] V. R. Taylor and L. L. Stowe. Reflectance characteristics of uniform earth and cloud surfaces derived from NIMBUS 7 ERB. *Journal of geophysical research*, 89:4987–4996, 1984.

[4] Patrick Minnis and Edwin F. Harrison. Diurnal variability of regional cloud and clear sky radiative parameters derived from goes data. part I: Analysis method. *Journal of climate and applied meteorology*, 23:993–1011, 1984.

[5] J. T. Suttles, Richard N. Green, Patrick Minnis, G. L. Smith, W. F. Staylor, Bruce A. Wielicki, I. J. Walker, D. F. Young, V. R. Taylor, and L. L. Stowe. Angular radiation models for Earth-atmosphere system. Reference publication 1184, NASA, July 1988. Volume I - Shortwave radiation.

[6] David R. Brooks, Edwin F. Harrison, Robert S. Kandel, Patrick Minnis, and John T. Suttles. Development of algorithms of understanding the temporal and spatial variability of the Earth's balance. *Review of Geophysics*, 24:422–438, May 1986.

[7] Jean-Philippe Duvel and Robert S. Kandel. Regional-scale diurnal variations of outgoing infrared radiation observed by METEOSAT. *Journal of climate and applied meteorology*, 24:335–349, April 1985.

[8] Dennis L. Hartmann and E. E. Recker. Diurnal variation of outgoing longwave radiation in the tropics. *Journal of climate and applied meteorology*, 25:800–812, 1986.

[9] Stephen A. Klein and Dennis L. Hartmann. Seasonal cycle of low stratiform clouds. *Journal of Climate*, 6:1587–1606, August 1993.

[10] Mark Adam Ringer. *Interannual variability of the Earth's radiation budget and cloudiness: A satellite view.* . PhD thesis, University of Reading, U.K., 1994.

[11] William B. Rossow, E. Kinsella, A. Wolf, and L.C. Garder. International satellite cloud climatology project (ISCCP) description of reduced resolution radiance data. Technical Report WMO/TD No. 58, World Meteorological Organisation, Geneva, 1987.

[12] Jean-Philippe Duvel. Analysis of diurnal, interdiurnal and interannual variations during northern hemisphere summers using METEOSAT infrared channels. *Journal of climate*, 1:471–484, May 1988.

[13] Bruce R. Barkstrom, Ed Harrison, G. Smith, Richard N. Green, J. Kibler, R. Cess, and the ERBE Science Team. Earth Radiation Budget Experiment ERBE archival and April 1985 results. *Bulletin of American Meteorological Society*, 70:1254–1262, 1989.

[14] William B. Rossow, L.C. Garder, B. Kachmar, Y.uanchong Zhang, and Alison W. Walker. *International satellite cloud climatology project (ISCCP) documentation of cloud data*. NASA Goddard Space Flight Center, New York, 1991.

[15] William B. Rossow, A. W. Walker, D. Beuschel, and M. Roiter. International satellite cloud climatology project (ISCCP): Description of new cloud data sets. Technical Report WMO/TD No. 737, World Climate Research Programme (IcSu and WMO, Geneva, February 1996.